Receiver-Based Experimental Estimation of Power Losses in Optical Networks

A. May, F. Boitier, E. Awwad, P. Ramantanis, M. Lonardi, P. Ciblat

Abstract— **We propose a method to estimate the amplitude of an unexpected power loss which, leveraging on a calibration, enables the real-time monitoring of a network link. It is based on an existing fiber-longitudinal power profile evaluation technique. The reliability of the method is assessed experimentally. When the anomaly is located at 0 km from the beginning of the span, the estimation bias is smaller than 0.2 dB for losses up to 10 dB. When the anomaly is located at 25 km from the beginning of the span, the same estimation bias is observed but for losses up to 5 dB. In both cases, the standard deviation of the estimation is smaller than 0.2 dB.**

I. INTRODUCTION

Optical communication systems were designed with large static margins to always ensure the target performance without any external intervention. Since system monitoring was limited or even non-existent, margins were considered to cover for inaccuracies of the optical system parameters and time-varying network conditions [1]. Recently, elastic monitoring-enabled networks promise to squeeze down margins and adapt the transmission to the network conditions.

To meet this expectation, affordable and reliable monitors were developed. Regarding the optical fiber parameters estimation, low-cost and accurate methods were proposed for characterizing the chromatic dispersion [2] or the non-linear parameter [3]. Moreover, to describe the time-varying network conditions, a polarization state monitoring method was proposed in [4]. In [5], it has been shown that the power attenuation uncertainty has a significant impact on the system characterization. Therefore, accurately estimating power losses –which may come from abnormal splicing, excessing connector loss, intrusion, or tapping– enables us to make the best possible decision in terms of operational cost or outage avoidance. Decisions may include repairment, rerouting (as in [4]), or a transmission parameters adjustment.

At the present day, one solution to estimate the location and the value of a power loss is the use of an optical time-domain reflectometer (OTDR) in adjacent bands. Although this technique is quite accurate, it often requires human intervention since it is rarely available at optical nodes because of its cost. For this reason, novel techniques able to estimate the longitudinal power profile by employing coherent receiver samples have been proposed in [6] and [7]. Their approach requires a dispersion-unmanaged optical link but does not need any additional hardware or propagation of adjacent signals. Both techniques enable the localization of power losses in multi-span links through an anomaly indicator (AI) function. While they both show a link between the value of the inserted loss and the AI, they do not focus on the loss estimation problem and on the possible accuracy of the estimation. This latter feature could eventually be accomplished by measuring the loss from the in-line optical amplifiers' inputs and outputs and by feeding it back to the transponders. Nevertheless, the acquisition and the distribution of these data would be rather expensive and should be avoided.

In this letter, based on the longitudinal power profile estimation technique developed in [6], we propose a calibration-based method to estimate the value of a power loss due to anomalies. The calibration is done at each span amplifier and enables the real-time monitoring of an optical link. We experimentally evaluate the accuracy of the loss amplitude estimation for a three-100km-span link.

The paper is organized as follows: in Section II, the experimental set-up is described. In Section III, the proposed method to estimate the loss location z_0 and the value of the loss l_{dB} -related to the transmission factor T_0- is introduced. In Section IV, experimental results are provided, showing the relevance of our method.

II. EXPERIMENTAL SET-UP

Fig. 1 depicts the experimental set-up. We consider a 300 km fiber link composed of three 100 km spans of single- mode fiber (SMF). Thirty 32 GBd dual-polarization (DP) quadrature phase-shift keying (QPSK) channels are used. The attenuation constant of the fibers is equal to $\alpha_{dB} = 0.206$ dB/km. The total cumulated chromatic dispersion of the link is 5100 ps/nm. The channel under test (CUT) is digitally pre-distorted with a cumulated chromatic dispersion (CD) of 3000 ps/nm. The launch power at every span is 5 dBm for the CUT and 0 dBm for each adjacent channel. Losses are inserted through variable optical attenuators (VOA) and are placed at three different locations: i) at 0 km, ii) at 25 km, or iii) at 50 km into the second span. The inserted losses may vary from 1.6 dB to 9.9 dB. The proposed method is based on samples acquired from the four real-valued outputs of the coherent receiver sampling at a rate of 200 GSamples/s.
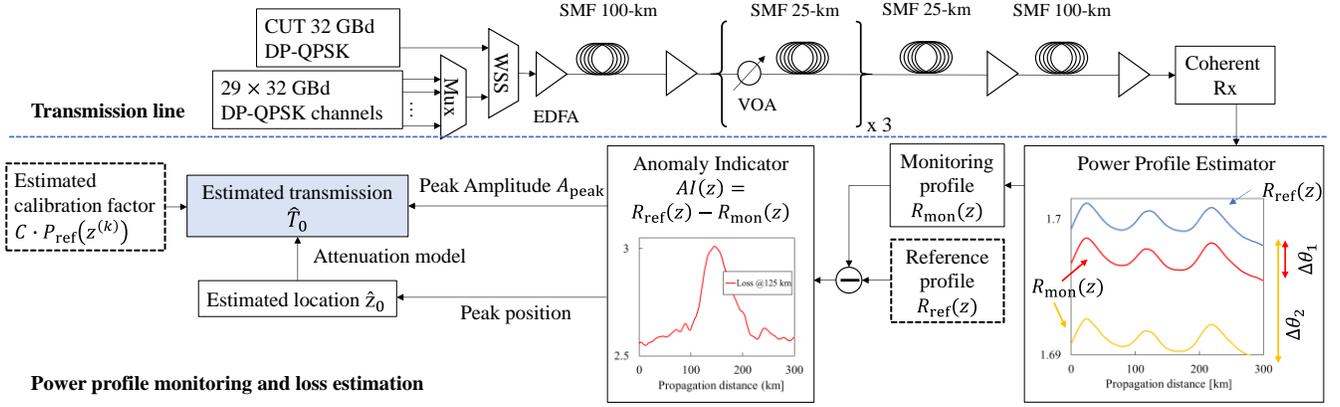
Fig. 1. Experimental set-up and proposed method scheme. CUT: channel under test, Mux: multiplexer, WSS: wavelength selective switching, EDFA: erbium-doped fiber amplifier, VOA: variable optical attenuator, SMF: single-mode fiber.

III. PROPOSED METHOD

Before introducing our method for estimating the loss amplitude, we briefly remind the estimation technique for the longitudinal power profiles described in [6]. This technique relies on the non-commutative relationship between the chromatic dispersion (CD) and the nonlinear self-phase modulation (SPM) along a fiber link of length L. Such a power profile, denoted by $R(z)$ where z is the propagation distance, is computed as the normalized correlation between the magnitudes of two signals noted y_1 and $y_2(z)$. The first signal y_1 is the reconstructed transmitted waveform (from the decoded bits). The second signal $y_2(z)$ is obtained in several steps. First, polarizations are demultiplexed. Second, the CD corresponding to a distance $L - z$ is compensated and a phase rotation of ϵ is performed to compensate for SPM effects partially. As in [6], ϵ is set to 0.01. Finally, the CD corresponding to the remaining distance z is compensated. In practice, we compute each $R(z)$ independently for each z. The granularity $\Delta z = L/N$, which depends on the number of points N of the profile, can be tuned. It is set to $\Delta z = 1$ km in this letter.

Our proposed method to estimate the value of a loss is summarized in the bottom part of Fig. 1. We first need a reference configuration that provides the reference power profile denoted by $R_{\text{ref}}(z)$. Then, during a second phase, we periodically monitor the power profile denoted by $R_{\text{mon}}(z)$. For example, one reference profile and two monitoring profiles – each with a different inserted power loss at 125 km– are plotted in Fig. 1, in the "power profile estimator" box. Finally, we compute the so-called anomaly indicator (AI) defined as [6]:

$$AI(z) = R_{\text{ref}}(z) - R_{\text{mon}}(z). \tag{1}$$

When a loss occurs, the AI function does not vanish and allows us to estimate its location z_0 and its amplitude l_{dB}. This latter quantity can be determined by finding and inverting the transmission factor T_0 through $l_{\text{dB}} = -10 \log_{10}(T_0)$. In the coming paragraphs, we go through the details for determining T_0.

At the present form, $R(z)$ is a normalized correlation and therefore, to evaluate T_0, we propose to correlate $R(z)$ to the power. We suggest an affine relationship between $R_i(z)$ and the optical power in the link $P_i(z)$ as follows:

$$R_i(z) = C \cdot P_i(z) + \theta_i, \tag{2}$$

where $i \in \{\text{ref}, \text{mon}\}$, $C > 0$ is a proportionality factor and θ_i is an offset factor. We assume that C is independent of the configuration, i.e., reference or monitoring, for a given link and given transmission parameters. The offset θ_i depends on the total accumulated noise. Since some noise contributions (ASE, SPM and cross-phase modulation XPM effects) depend on the configuration, so does θ_i. Consequently, injecting (2) into (1) leads to:

$$AI(z) = C \cdot \left(P_{\text{ref}}(z) - P_{\text{mon}}(z) \right) + \Delta\theta, \tag{3}$$

with $\Delta\theta = \theta_{\text{ref}} - \theta_{\text{mon}}$. Let k be the index of the span in which the anomaly occurs and $z^{(k)}$ the beginning of this span. If this loss is located at z_0, the power $P_{\text{mon}}(z)$ at a given point $z > z_0$ and up to $z^{(k+1)}$, is multiplied by a transmission factor $T_0 < 1$. At $z^{(k+1)}$, we assume the amplifier compensates for the total losses of the previous span. Hence, we can express $P_{\text{mon}}(z)$ as:

$$P_{\text{mon}}(z) = \begin{cases} P_{\text{ref}}(z), & 0 \le z < z_0 \\ T_0 \cdot P_{\text{ref}}(z), & z_0 \le z < z^{(k+1)} \\ P_{\text{ref}}(z), & z^{(k+1)} \le z < L. \end{cases} \tag{4}$$

Combining (3) and (4) implies that:

$$AI(z) = \begin{cases} \Delta\theta, & 0 \le z < z_0 \\ C \cdot (1 - T_0) \cdot P_{\text{ref}}(z) + \Delta\theta, & z_0 \le z < z^{(k+1)} \\ \Delta\theta, & z^{(k+1)} \le z < L. \end{cases} \tag{5}$$

As $\Delta\theta$ depend on several parameters, including T_0 as shown in Fig. 1, we will focus our analysis directly on the peak amplitude A_{peak} of the AI function given by:

$$A_{\text{peak}}(z_0, T_0) = \max_{0 < z < L} \left(AI(z) \right) - \Delta\theta \tag{6}$$
$$= C \cdot (1 - T_0) \cdot P_{\text{ref}}(z_0)$$

From (6), we can see that A_{peak} is directly proportional to the loss factor $(1 - T_0)$.

To obtain T_0 from A_{peak}, we need to determine C and $P_{\text{ref}}(z_0)$. To determine the latter coefficient, we propose to rely on the following attenuation model:

$$P_{\text{ref}}(z_0) = P_{\text{ref}}(z^{(k)}) \cdot 10^{-\alpha_{\text{dB}} \cdot \frac{z_0 - z^{(k)}}{10}} \tag{7}$$

where α_{dB} is the fiber attenuation constant in dB/km. Injecting (7) into (6), we finally obtain:
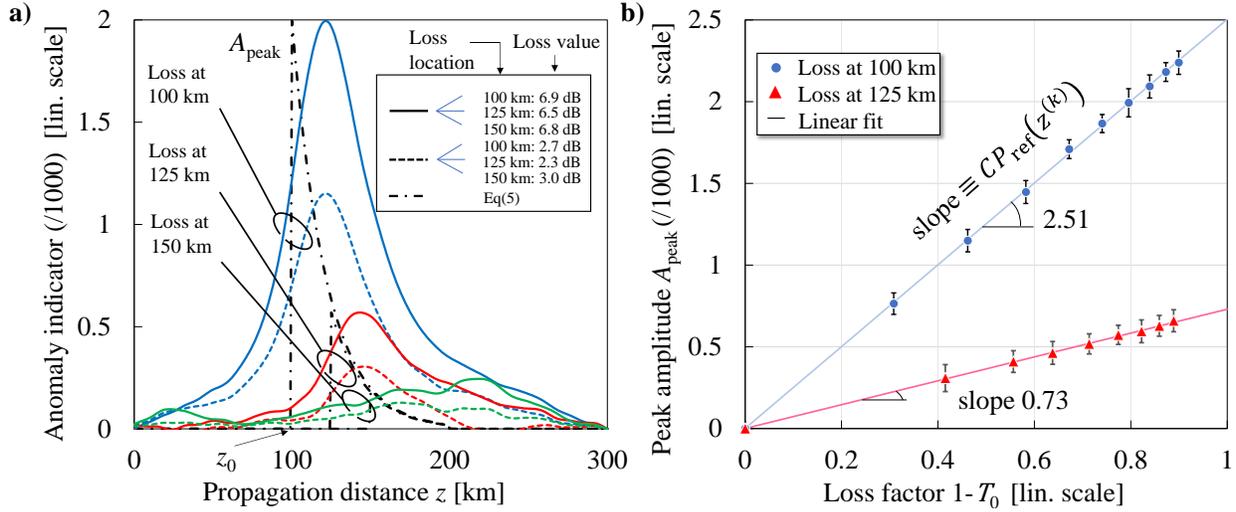
Fig. 2. Experimental results. a) Anomaly indicators minus $\Delta\theta$ versus the propagation distance in km for different values of loss located at three different locations b) Values of AI peak amplitude versus the loss factor $(1 - T_0)$.

$$A_{\text{peak}}(z_0, T_0) = \quad (8)$$

$$C \cdot (1 - T_0) \cdot P_{\text{ref}}(z^{(k)}) \cdot 10^{-\alpha_{\text{dB}} \cdot \frac{z_0 - z^{(k)}}{10}}$$

To evaluate $C \cdot P_{\text{ref}}(z^{(k)})$, we will perform a calibration step. This calibration is done by modifying the output power of the amplifier at the beginning of the kth span. This modification can be seen as a loss factor $(1 - T_0)$ applied at $z_0 = z^{(k)}$ in (8). Thus, we can extract the slope value $C \cdot P_{\text{ref}}(z^{(k)})$ thanks to a linear regression. This calibration step also allows for the determination of the position of the beginning of the span of interest $z^{(k)}$.

To further use our calibration value and finally access to the value of losses anywhere along the fiber, according to (8), we need to estimate the loss position with respect to the amplifier location $z_0 - z^{(k)}$. According to [6], those two positions are given by the position of the maximum of the rising slope of the peak, i.e., the maximum of the derivative of the AI. Since we only need to determine the loss position with respect to the amplifier location, it is sufficient and possible to take the relative position of the maximum of the two AI peaks, one given by the calibration and the other during the monitoring stage.

In the following, we confirm through experiments that (5) and (8) hold. According to the experimental set-up described in Section II, the measured AIs versus the propagation distance z for different loss factors (expressed in dB) and loss locations, are plotted in Fig. 2a. We choose to remove $\Delta\theta$ from each of the AI to enable us to easily compare the curves. In addition, (5) is plotted for each loss location and their considered maximum loss value. As in [6], we remark that the loss location is closer to the maximum rising slope than the peak location. We also observe that the peak amplitude is an increasing function of the loss, as expected with (5). However, the peak amplitude for a given loss is a decreasing function of the loss location as expected with (8). There is thus a fair agreement between (5) and the experimental measurements. Note that the AI are not equal to a constant in the third span, compared to (5), due to the significant width of the peaks.

In Fig. 2b, we plot the peak amplitude versus $(1 - T_0)$ for different loss locations. Based on 20 trials, 3σ-error bars are added, and two linear regressions are drawn. We observe that

the linear regressions confirm the T_0-dependence of (8). A calibration factor of 2.51 is determined from the slope of the 100km case. The slope determined at 125 km is 0.73, not far from $2.51 \cdot 10^{-\alpha_{\text{dB}} \cdot \frac{25\text{ km}}{10}} = 0.77$, confirming the relevance of the attenuation model. Consequently, (8) applies and we confirm that the AI metric and its peak are suitable choices for estimating our parameters of interest.

Nevertheless, since A_{peak} decreases exponentially with z_0, the peak may be harder to detect and estimate if the loss is far away from the amplifier (see the 150-km case in Fig. 2a).

IV. EXPERIMENTAL PERFORMANCE

Here, we assess the experimental performance of the proposed method. To compute AI, we need an estimate of the power profiles. Each power profile (the reference and the monitoring ones) is obtained by averaging N_p elementary power profiles. The correlations involved in each elementary profile are estimated using a sequence of N_s samples where the sampling rate is twice the symbol rate. Here, $N_s = 2048$. In (6), $\Delta\theta$ is replaced with a rough estimate given by $AI(L)$. In Fig. 3a, we plot the standard deviation of the estimated $\hat{l}_{\text{dB}}$ versus N_p for different values l_{dB} of inserted losses located at 125 km. Each standard deviation is computed thanks to 20 trials, i.e., 20 estimated $\hat{T}_0$. It highly decreases with N_p until reaching an asymptote above $N_p = 20000$. Depending on the accuracy needed, by the alarm threshold for instance, the value of N_p can be adapted accordingly. Notice that Fig. 2a and Fig. 2b have been plotted with $N_p = 20000$ and $N_p = 3000$ respectively. $N_p = 3000$ has been chosen in Fig. 2b to see the error bars.

In Figs. 3b-i and ii, we plot the estimated losses $\hat{l}_{\text{dB}}$ versus the inserted losses l_{dB} with 3σ-error bars at 100 and 125 km, respectively. The mean value corresponds to the circle point, and each bar has been obtained thanks to 30 estimated losses $\hat{l}_{\text{dB}}$. The estimation is very accurate when the loss is located at the output of the amplifier for all inserted losses. For losses located at 125 km, the estimation bias is smaller than 0.2 dB, as well as the standard deviation, for inserted losses up to 5 dB. For higher inserted losses, both the estimation bias and the standard deviation are larger. This is mainly due to localization
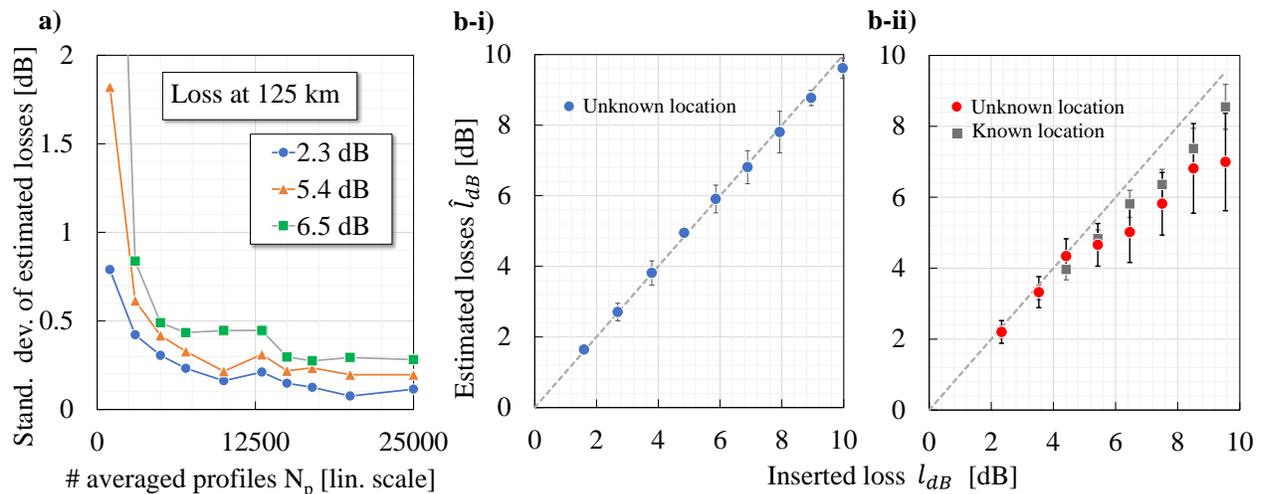
Fig. 3. Experiments. a) Standard deviation of the estimated loss. b) Estimated versus inserted loss at i) 100 and ii) 125 km. Dashed line : inserted loss. Markers: estimation.

errors. Indeed, by also plotting $\hat{l}_{dB}$ –with squares– and its 3σ-error bars when the location is known, we observe that the bias is reduced and the standard deviations are smaller than when the location is unknown and estimated with the *AI* peak positions. This remaining bias is mostly due to the difference between the calculated slope at 125 km from the calibration factor and the actual slope given by the linear regression, a difference which was mentioned at the end of Section III.

To generalize our experimental results and more particularly the calibration to other set-ups, we perform a set of simulations to see the impact of the symbol rate. All simulation parameters except the symbol rate are identical to the ones described in Section II. For simplicity, we consider a single-channel field. In Fig. 4, we plot the normalized peak amplitude versus $(1 - T_0)$ for various symbol rates but constant power with $z_0 = z^{(2)}$, i.e., the loss located at the beginning of the second span. By normalized peak amplitude, we mean A_{peak} divided by the value of $C \cdot P_{\text{ref}}(z^{(2)})$ computed for the 32 GBd case. Once again, we remark that the peak amplitude is proportional to $(1 - T_0)$ validating (8). However, the slopes are different, which implies that the calibration factor is different for each
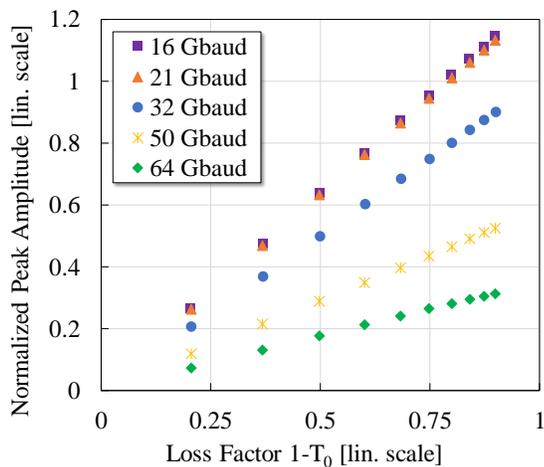
symbol rate. Hence, if multiple symbol rates are to be used, a look-up table is required to profile all transmission modes.

V. CONCLUSION AND PERSPECTIVES

We proposed a simple method for monitoring a link by estimating the value of an unexpected power loss. We showed with experiments that the method offered an accurate estimate. Consequently, we advocate its use for real-time monitoring in WDM systems. The performance should indeed not be much dependent on the wavelength in the C-band as well as on the number of channels since we are mainly exploiting the intra-channel effects. However, when the loss is close to the end of the span, because of small peak amplitudes, new algorithms should be developed to exhibit an accurate estimate from *AI*.

Fig. 4. Simulations results. AI peak amplitudes for different symbol rates for a loss located at 100 km.

REFERENCES

[1] Y. Pointurier, 'Design of Low-Margin Optical Networks', *J. Opt. Commun. Netw.*, vol. 9, no. 1, p. A9, Jan. 2017, doi: 10.1364/JOCN.9.0000A9.

[2] C. Malouin, M. Arabaci, P. Thomas, B. Zhang, T. Schmidt, and R. Marcoccia, 'Efficient, Non-Data-Aided Chromatic Dispersion Estimation via Generalized, FFT-Based Sweep', in *Optical Fiber Communication Conference/National Fiber Optic Engineers Conference 2013*, Anaheim, CA, 2013, p. JW2A.45, doi: 10.1364/NFOEC.2013.JW2A.45.

[3] L. Jiang *et al.*, 'Chromatic Dispersion, Nonlinear Parameter, and Modulation Format Monitoring Based on Godard's Error for Coherent Optical Transmission Systems', *IEEE Photonics J.*, vol. 10, no. 1, pp. 1–12, Feb. 2018, doi: 10.1109/JPHOT.2017.2786697.

[4] F. Boitier *et al.*, 'Seamless Optical Path Restoration with Just-in-Time Resource Allocation Leveraging Machine Learning', in *2018 European Conference on Optical Communication ECOC*, Rome, Sep. 2018, pp. 1–3, doi: 10.1109/ECOC.2018.8535279.

[5] P. Ramantanis, C. Delezoide, P. Layec, and S. Bigo, 'Revisiting the calculation of performance margins in monitoring-enabled optical networks', *J. Opt. Commun. Netw.*, vol. 11, no. 10, p. C67, Oct. 2019, doi: 10.1364/JOCN.11.000C67.

[6] T. Tanimura, S. Yoshida, K. Tajima, S. Oda, and T. Hoshida, 'Fiber-Longitudinal Anomaly Position Identification Over Multi-Span Transmission Link Out of Receiver-end Signals', *J. Lightwave Technol.*, vol. 38, no. 9, pp. 2726–2733, May 2020, doi: 10.1109/JLT.2020.2984270.

[7] T. Sasai *et al.*, 'Simultaneous Detection of Anomaly Points and Fiber types in Multi-span Transmission Links Only by Receiver-side Digital Signal Processing', in *Optical Fiber Communication Conference (OFC) 2020*, San Diego, California, 2020, p. Th1F.1, doi: 10.1364/OFC.2020.Th1F.1.